Journal of The Electrochemical Society

OPEN ACCESS

Quantifying the Effect of Separator Thickness on Rate Performance in Lithium-Ion Batteries

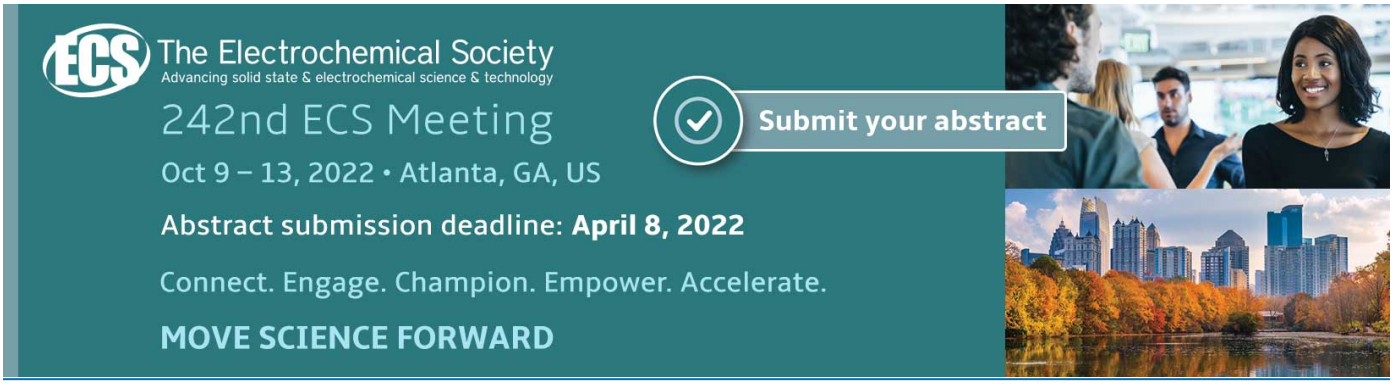

Journal of The Electrochemical Society, 2022 **169** 030503

Quantifying the Effect of Separator Thickness on Rate Performance in Lithium-Ion Batteries

Dominik V. Horváth,[1] Ruiyuan Tian,[1] Cian Gabbett,[1] Valeria Nicolosi,[2] and Jonathan N. Coleman[1,z]

[1]*School of Physics, CRANN & AMBER Research Centres, Trinity College Dublin, Dublin 2, Ireland*
[2]*School of Chemistry, CRANN & AMBER Research Centres, Trinity College Dublin, Dublin 2, Ireland*

In addition to improving parameters such as energy density and stability, it is important to maximise rate performance in lithium-ion batteries. While much work has focused on rate-limiting factors associated with the electrodes, much less attention has been paid to the effect of the separator on rate-performance. Here we perform a quantitative study on the effect of separator thickness on the rate-performance of a model system of NMC-based half cells. By fitting experimental capacity vs rate curves, we measured the characteristic time associated with charge/discharge as a function of separator thickness, finding a roughly linear increase for separator thicknesses below ~65 μm. This behaviour is consistent with a simple physical model which shows the separator thickness dependence to be dominated by electrolyte resistance effects. The predictions of the model match the data extremely well with no adjustable parameters.
 [DOI: 10.1149/1945-7111/ac5654]

Manuscript submitted November 23, 2021; revised manuscript received February 3, 2022. Published March 9, 2022.

Supplementary material for this article is available online

Rechargeable Li-ion batteries contain a pair of electrodes isolated from each other by a separator membrane.[1–3] These porous components usually consist of polymeric materials, with commercial batteries primarily using polyolefin separators.[3,4] Separator structure is often characterised by porosity (typically 40%–60%),[3,4] tortuosity (typically 2.5–4.5),[3,5–10] and pore size (<1 μm).[4] Within the battery, the porous interior of the separator is soaked with electrolyte, facilitating the back and forth movement of Li ions between the electrodes. The insulating electronic nature of the separator prevents electrons from moving through it, which are instead forced to travel through the current collectors attached to the electrodes. Hence, a separator needs to be highly conductive for Li ions, unpassable for electrons and thick enough to prevent short circuits. There are further properties which need consideration based on application, including thermal stability, electrolyte wettability, and resistance to chemical and physical degradation.[1]

Since a separator does not contribute towards energy storage, maximising energy density within the cell requires the separator volume to be minimised, while retaining its core functionality.[1,2] Practically, this is achieved by minimising separator thickness. Achieving this also reduces the resistance of the electrolyte within the separator and indeed the time associated with diffusion of ions across the separator. These factors are of specific interest to this paper because it is well known that such effects benefit the rate performance of cells.[3,11]

While some papers have described the gains in rate performance associated with reduced separator thickness, these are qualitative observations.[12–15] Quantitative results appear to be very limited. Recently, Horvath et al. showed that the effect of electrode on rate performance is slightly modified by changing separator thickness.[16] On the other hand, Miranda et al. used a modified version of the Doyle/Fuller/Newman model to simulate the effects of separator thickness on rate performance.[17,18] For a model system with 70% porosity and a tortuosity of 3.8, they found that rate performance (0.15–5 C test range) is unaffected by separator thicknesses in the range 1–32 μm. However, this result is somewhat inconclusive because the electrode thickness does not appear to be given in the paper. If the electrode under study was very thick, one would expect the relative effect of the separator to be very limited.[16,19] It would seem that a comprehensive quantitative study on the effect of separator thickness on rate performance is needed.

Recently, we reported a simple, semi-empirical equation which can be used to fit capacity vs rate (i.e. current) data which yields the characteristic time, τ, associated with charging/discharging of the cell.[19] Using this procedure to obtain τ makes it simple to quantify the effect of various parameters on rate performance. In addition, we reported a physical model which quantifies how various rate-limiting factors contribute to τ. The model describes the rate limitations occurring within the battery via diffusive, capacitive (electrical) and electrochemical contributions and results in a simple equation (see below) which expresses τ in terms of factors such as electrode and electrolyte conductivity, solid and electrolyte diffusivity as well as dimensional parameters. To date, we have shown comprehensively that data for τ as a function of electrode thickness (L_E) and out-of-plane electrical conductivity (σ_{OOP}) of the electrode are perfectly in line with the predictions of the model.[16,20] Among the parameters included in the model is the separator thickness, L_S, with the equation predicting that τ varies with separator thickness via terms involving L_S and L_S^2. We believe it is of interest to experimentally measure τ for various separator thicknesses to obtain empirical evidence of the impact of separator thickness on rate performance. Such data could of course be compared to the predictions of our (or indeed any other) model. Such an approach would improve our understanding of the relationship between separator thickness and rate performance and if good agreement were found, would provide additional validation to the model.

In this work, we studied the properties of a model half-cell system with varying separator thicknesses (L_S = 16–144 μm). We first used impedance spectroscopy to characterise the electrolyte resistance as a function of separator thickness, obtaining the conductivity of the electrolyte within the separator. We then used chronoamperometry[20] (CA) to characterise the rate performance of NMC-based lithium-ion half cells as a function of separator thickness and obtained τ by fitting. We show that the τ vs L_S data is consistent with our model. In addition, we find that the effect of separator thickness on rate performance to be dominated by electrolyte resistance effects and to be consistent with results from impedance spectroscopy.

Experimental

Electrode preparation.—All electrodes were prepared via the conventional slurry-casting method. $LiNi_{0.5}Mn_{0.3}Co_{0.2}O_2$ (NMC,

[z]E-mail: colemaj@tcd.ie

MTI Corp.) powder was mixed with a dispersion of single-walled carbon nanotubes (CNTs) in N-Methyl-2-pyrrolidone (NMP) (0.4 wt% CNT in NMP, 2 wt% Polyvinylidene fluoride (PVDF) as surfactant stabilizer, Tuball, OCSiAl). This slurry was homogenised using a mortar and pestle and cast onto an Al current collector using a doctor blade. Residual NMP was evaporated from the films by drying at 40 °C overnight. This low temperature is required to avoid cracking in the NMC/CNT composite films.[16,20–22] Once NMP was evaporated, the CNT mass loading was 0.5 wt% and the areal active mass loading was ~5 mg cm^{-2}. The films were then calendered until a density of ~2 g cm^{-3} was reached, corresponding to electrodes with thicknesses between 25–30 μm. The morphology of the NMC/CNT electrodes and stacked layers of battery separators were examined using scanning electron microscopy (SEM). An accelerating voltage of 2–5 keV was used with a 30 μm aperture at a working distance of 5–6 mm (Zeiss Ultra Plus).

Electrochemical measurements.—The electrochemical performance of the NMC/CNT electrode was evaluated in half-cell configuration using CR2032 (MTI Corp.) coin-cells. The electrode was cut into circular discs (diameter = 1.2 cm, geometric area=A_0 = 1.13 cm^2) and acted as the working electrode. L_S was varied by stacking multiple layers (N = 1–9) of separators (Celgard C212, L_S = 16 μm) within the cell. We make the assumption that the tortuosity of the stack is the same as the tortuosity of the individual separators. Separators were individually added to the stack and a small amount of electrolyte was dropped on each new separator to ensure complete electrolyte absorption. 1.2 M $LiPF_6$ in ethylene carbonate/ethyl methyl carbonate (EC/EMC, 1:1 in v/v, BASF) with 10 wt.% fluoroethylene carbonate (FEC) was used as the electrolyte. Li metal was used as the counter electrode and the coin-cells were assembled in an Ar-filled glovebox (UNIlab Pro, Mbraun), with O_2 and H_2O levels <0.1 ppm. During cell assembly, the sealing pressure (~8 MPa) was set to be the same for all cells and all separator thicknesses. Given that the compressive modulus of a PP separator is ~1 GPa, this pressure should lead to negligible deformation (<1% compression) in all cases.

The assembled cells were evaluated using galvanostatic charge-discharge (GCD) measurements (BioLogic VMP-3). Five initial charge-discharge cycles (between 3.6–4.5 V at 16 mA g^{-1}) were performed to activate the cells. After stable capacities (capacity change <1%) and a Coulombic efficiency of >99% was reached, the cells were charged to 4.5 V at 16 mA g^{-1}. To determine the ionic conductivity of the electrolyte within the separator, separate CR2032 coin cells were prepared. In these cells, a stainless-steel spacer replaced the NMC/CNT electrodes, and EIS was used to record the electrolyte resistance ($R_{Electrolyte}$). EIS was performed in the 1 MHz–1 Hz frequency region with a 10 mV voltage amplitude (BioLogic VMP-3). The electrolyte resistance was determined from the first intercept of the real impedance (Re(Z)) axis on Nyquist plots. Lastly, cyclic voltammetry (CV) was conducted on a separate NMC/CNT half-cell in the voltage range of 3.6–4.5 V at scan rates of 0.1, 0.5, 1 and 2 mV s^{-1}.

Rate performance was analysed using the CA method, as previously reported by us[20] and and Heubner et al.[23] CA was performed by applying the lower cut-off potential (3.6 V) for 7 h and three to four charged NMC/CNT half-cells were used for each L_S value. Subsequent current transients were converted to specific capacity (Q/M, normalised to active mass) vs rate (R) curves using the following equations:[20,23]

$$\frac{Q}{M} = \int_0^t (I/M)\,dt$$

$$R = \frac{I/M}{Q/M}$$

where I/M is the specific current, Q/M is the experimentally measured specific capacity (at a given I/M) and t is the timeframe given by the current transient.

Results and Discussion

Electrode materials.—To quantitatively investigate the effects of separator thickness on rate performance we chose $LiNi_{0.5}Mn_{0.3}Co_{0.2}O_2$ (NMC) as a model active material for its high usable discharge capacity and good rate capability.[24] We combined NMC with 0.5 wt% single-walled carbon nanotubes (CNTs), so that the CNTs fulfil the roles of both the binder and the conductive additive. This type of composite has been shown to yield robust electrodes that are capable of achieving high specific capacities even at large electrode thicknesses.[21] The cathodes were tested in half-cell configurations, with Li metal as the counter electrode. The separator thickness, L_S, was varied by stacking multiple separators within the cells, giving an L_S range of 16–144 μm.

The morphology of the NMC/CNT cathodes was investigated using SEM. The typical structure is shown in Fig. 1A, where larger, spherical NMC secondary particles (~20 μm) are enveloped in a network of CNTs. This structure is known as a segregated network, one that arises when CNTs are forced to wrap around larger particles. The benefits of this network are high electronic conductivity (out of plane conductivity was measured to be ~0.17 ± 0.06 S m^{-1} for our electrodes), increased robustness and large low-rate capacities that approach the theoretical value.[21,25,26] Figure 1B shows a magnified image of a secondary particle with several attached CNTs wrapping around it and confirms the NMC secondary particles to be made up of smaller primary particles (710 ± 20 nm diameter averaged over 100 particles).

The electrochemical performance of the cells was tested using CV and GCD measurements. The cells were first activated by running five charge-discharge cycles (16 mA g^{-1}, 3.6–4.5 V) using GCD to ensure solid-electrolyte interphase (SEI) formation. The voltage profile of a typical cell extracted from the second charge-discharge cycle of activation is shown in Fig. 1C. At 16 mA g^{-1}, the NMC/CNT cathode delivers ~170 mAh g^{-1} discharge capacity, in line with NMC materials at similar voltage ranges.[27] Additionally, we conducted CV on a separate cell at various scan rates in the same voltage range. Voltammograms are shown in Fig. 1D, where the cathodic peak at 3.69 V corresponds to Li^+ insertion and the anodic peak at 3.83 V indicates Li^+ extraction.[28] To investigate the cyclability of the electrodes, we cycled a typical cell for 25 cycles at 16 mA g^{-1} (Fig. 1E). The specific discharge capacity remains steady over the 25 cycles, with an average value of 170.0 ± 0.6 mAh g^{-1}. As the NMC/CNT electrodes display high and stable specific capacities, we believe that they are a suitable model system for the investigation of separator thickness on rate performance.

Varying separator thickness.—The main aim of this paper is to quantitatively investigate the effect of varying separator thickness, L_S, on the rate performance of our model system. The separator thickness was varied by stacking multiple (up to 9) 16 μm thick separator membranes, giving an L_S-range of 16–144 μm. In Fig. 2A, four layers of separators are stacked and imaged from the side using SEM. While each individual layer has a mean thickness of 16 μm, in Fig. 2A the edges appear thicker due to the cutting process curling the edges of the sheets.

The most basic effect of changing the separator thickness is its impact on the resistance of the electrolyte within the porous interior of the separator. This effect was evaluated using EIS. For this purpose, we prepared a set of dummy-cells where the NMC/CNT electrodes were replaced with stainless steel current collectors and the separator thickness was varied by stacking one to nine separators (see Experimental for full details). The impedance spectra of two representative cells (L_S = 16 μm and 128 μm) are shown on a Nyquist plot, in Fig. 2B. $R_{Electrolyte}$ can be found from the intercept with the Re(Z) axis which occurs at high frequency. This graph shows that $R_{Electrolyte}$ shifts to higher resistance values with higher L_S. This trend is explained by the increased path lengths that the ions take through the separator.

To determine the conductivity of the electrolyte within the porous interior of the separator, σ_S, we plot $R_{Electrolyte}$ as a function of L_S

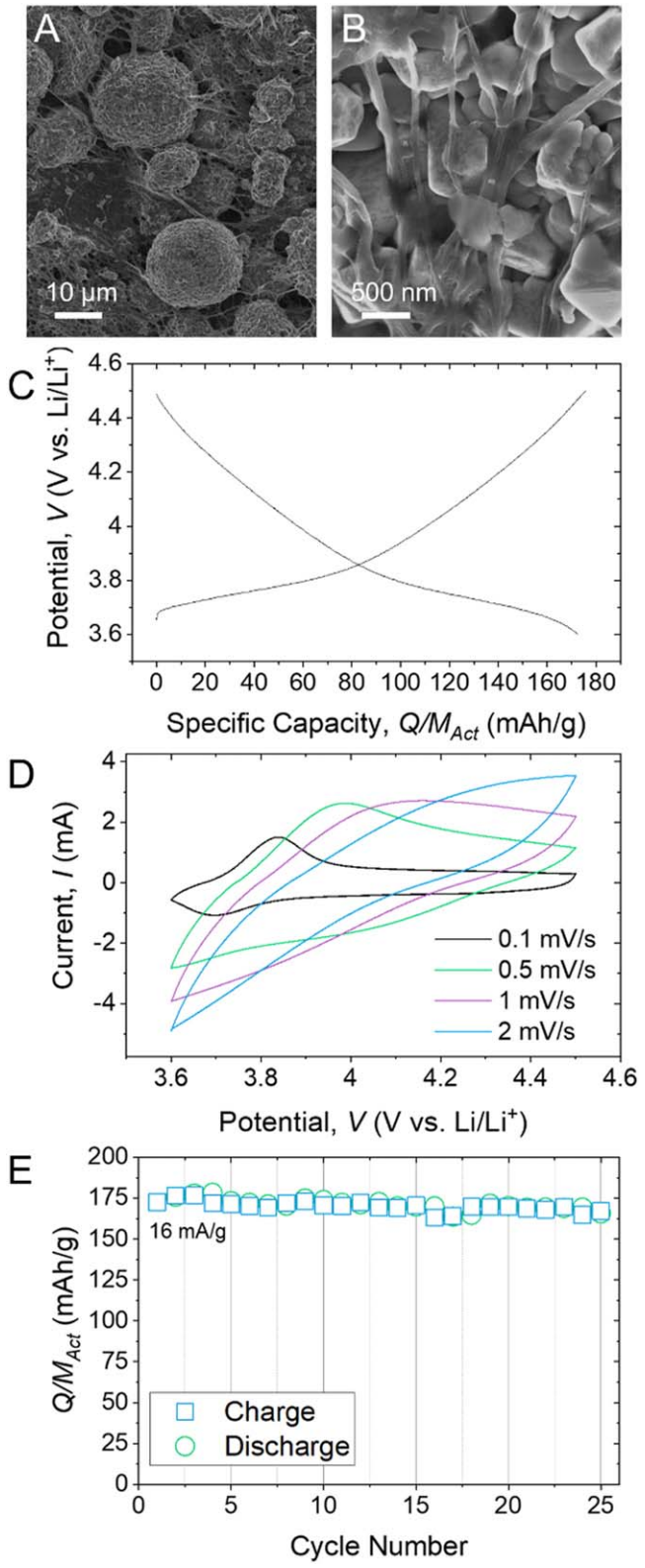

Figure 1. (A)–(B) Low- and high-magnification SEM images of an NMC/CNT (0.5 wt%) segregated network cathode. (A) Secondary particles enveloped by the nanotube network and (B) primary particles making up the secondary particles. (C)–(E) Electrochemical performance of the NMC/CNT model system as Li battery cathodes. Various tests conducted in half-cell configuration with a separator thickness (L_S) of 16 μm. (C) Voltage profile during half-cell activation, (D) steady-state cyclic voltammetry performed at various scan rates and (E) low-rate cycling performance at 0.1C = 16 mA g^{-1}.

(Fig. 2C). Although there is some scatter, we see a clear increase of $R_{\text{Electrolyte}}$ with L_S over the thickness range examined. We expect $R_{\text{Electrolyte}}$ to given by:

$$R_{Electrolyte} = R_{Series} + \frac{L_S}{A_S \sigma_S} \quad [1]$$

where R_{Series} is due to contact resistances between cell components and the wires. The second term can be described as the ionic resistance due to the separator, which we can express using σ_S, L_S and the cross-sectional area of the separator, A_S. Fitting Eq. 1 to the data in Fig. 2C, we obtain $dR_{\text{Electrolyte}}/dL_S = (9.7 \pm 1.7) \times 10^4\ \Omega\ m^{-1}$. Using $A_S = 2.54 \times 10^{-4}\ m^2$, we find $\sigma_S = 0.04 \pm 0.01\ S\ m^{-1}$.

We can relate the experimentally determined σ_S value to its bulk-liquid counterpart, σ_{BL}, via the Bruggeman equation: $\sigma_S = \sigma_{BL} P_S/\kappa_S$, where P_S is the porosity of the separator and κ_S is the tortuosity factor of the separator.[29,30] For our electrolyte we expect $\sigma_{BL} = 0.5\ S\ m^{-1}$ which means that the data implies $\sigma_S/\sigma_{BL} = P_S/\kappa_S \approx 0.08$.[31] For the separators used here, the manufacturer specifies the porosity to be $P_S = 0.35$ in line with the results of our density measurements which yielded $P_S = 0.36 \pm 0.02$ (for density measurements, see Supplementary Note 1, for a schematic of the separator used in this work see Fig. S1 (available online at stacks.iop.org/JES/169/030503/mmedia)). Combining these values with the Bruggeman equation yields a tortuosity factor of $\kappa_S = 4.4$ which is within the expected range of 2.5–4.5[10] and agrees with those of Cannarella et al. who measured the tortuosity factors of two comparable trilayer Celgard separators, 2320 and 2340, at 4.5 and 3.9, respectively.[10]

Rate measurements.—The rate performance data of our NMC/CNT half-cells was acquired from chronoamperometric current transients as described in Ref. 20. We recorded current transients for cells with L_S between 16 and 144 μm and converted the data to specific capacity (Q/M) vs charge/discharge rate (R) as described in Methods. We note that R is defined as $R = (I/M)/(Q/M)$, where I/M is the specific current and Q/M is the experimental specific capacity measured at a given I/M value (for full details see the Experimental and Ref. 20). Calculating rate this way, as opposed to the conventionally-used C-rate, means that R^{-1} is a measure of actual charge/discharge time (at that current) as opposed to some notional time that might only apply at low-rate, as is the case with C-rate.[16]

Q/M vs R curves for three different L_S values are presented in Fig. 3A. As demonstrated before,[16,20] CA data gives a much more data-dense representation of rate performance when compared to traditional GCD measurements, with information available down to very low-rates. It is clear from this data that cells with thinner separators display higher specific capacity at higher rates. This confirms that rate performance improves as the separator gets thinner, behavior which has long been qualitatively known.[3,11] However, such experimental data is generally not quantitatively analysed. In the next section, we will use the models described above to perform such a quantitative analysis.

Fitting capacity-rate data.—Although other semi-empirical fitting equations exist which can fit Q/M vs R data,[32] we tend to use the equation proposed by Tian et al.,[20] largely because it has been successfully used to fit a wide range of published data:[19,33]

$$\frac{Q}{M} = Q_M[1 - (R\tau)^n(1 - e^{-(R\tau)^{-n}})] \quad [2]$$

Here, Q/M is the measured specific capacity (mAh g^{-1}, here normalised to active mass) and R is the rate ($R = (I/M)/(Q/M)$) while Q_M (mAh g^{-1}), τ (s) and n are fitting parameters.

The most important fitting parameter is τ, the characteristic charge/discharge time mentioned above. It's practical importance stems from the fact that it quantifies the threshold rate, R_T, the point where rate performance begins to fall off.[34] For instance, if we choose R_T to correspond to the point where specific capacity has

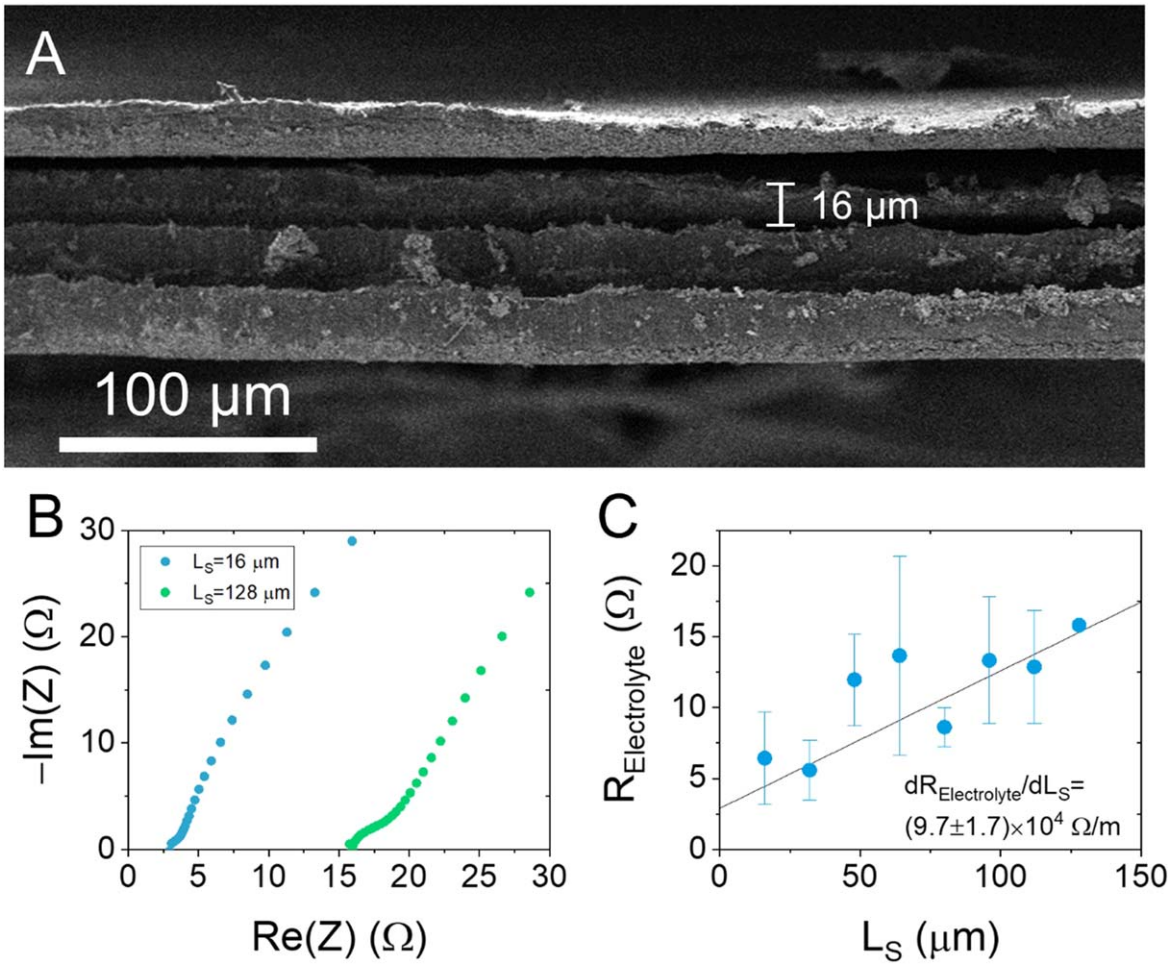

Figure 2. Properties of the separator stack. (A) Cross-sectional SEM image of four stacked separators. Each separator is 16 μm thick, however the edges of the separators appear larger due to curling caused by the cutting process. (B)–(C) Determination of ionic conductivity (σ_S) within the separator stack using EIS. (B) Nyquist plots of thin (N = 1) and thick (N = 8) separator stacks. $R_{Electrolyte}$ is determined from the high frequency Re(Z) intercept. (C) Electrolyte resistance as a function of separator thickness. The slope ($dR_{Electrolyte}/dL_S$) is used to calculate σ_S using Eq. 1.

fallen to 90% of its maximum value, then $R_T = (0.1)^{1/n}/\tau$ (see Fig. 3A). Below, we will focus on analysing the L_S-dependence of τ.

The exponent, n gives information about how quickly capacity decays at high rate. The value of n is thought to be $n \sim 0.5$ for electrodes with diffusion limitations and $n \sim 1$ for electrodes with electrical limitations.[19] Finally, Q_M is the specific capacity at extremely low rate and is a measure of the maximum possible performance. We note that for GCD data, the best way to obtain the low-rate specific capacity is by fitting to Eq. 1 to obtain Q_M. However, the availability of CA data at very low rates allows us to simply read-off the low-rate specific capacity ($Q/M_{Low\text{-}rate}$) from the low-rate plateau of Q/M vs R curves.[16]

First, we examine the trend of the low-rate specific capacity, $Q/M_{Low\text{-}rate}$, which is plotted against L_S in Fig. 3B. The data shows $Q/M_{Low\text{-}rate}$ to be constant in our L_S range, at 173.4 ± 1.8 mAh g^{-1}. In addition, we measured the measured electrode densities (close to 2 g cm^{-3} in all cases) to calculate the low-rate volumetric capacity ($Q/V_{Low\text{-}Rate}$) of the electrodes, which is plotted against L_S in Fig. 3B inset. We find $Q/V_{Low\text{-}Rate}$ also stays constant over the L_S range, with a mean value of $\langle Q/V_{Low\text{-}Rate}\rangle = 349 \pm 67$ mAh cm^{-3}.

Next, we used Eq. 2 to fit the Q/M vs R data for all 29 electrodes (L_S = 16–144 μm, see Fig. S2 for all fits). The fit parameters n and τ are plotted against separator thickness in Figs. 3C–3D. Here, each n and τ value (at a given L_S) is the average derived from three to four separate half-cell measurements, the error bar indicates the corresponding standard deviation. As shown in Fig. 3C, we find the exponent n to increase slightly from the value of 0.7 for a single separator (L_S = 16 μm) to ~0.8 for L_S = 64 μm before saturating somewhat. Because $n = 0.5$ is expected to represent diffusion limited behaviour while $n = 1$ represents electrically limited behaviour, such in increase may represent the effect of increasing electrolyte resistance as L_S is increased.

Most importantly, Fig. 3D shows τ to increase approximately linearly with L_S until $L_S \sim 65$ μm, above which it saturates at ~600 s. As τ is inversely proportional to R_T, the trend in Fig. 3C shows that rate performance is getting worse for cells with thicker separators as expected. Below, we will analyse this data in more detail using the physical model described above.

Quantitative analysis of τ vs L_S data.—As described above, the characteristic time, τ, increases with L_S, consistent with worsening rate performance. The initial increase is roughly linear with a slope of 5.8 × 10^6 s m^{-1} and an extrapolated zero-L_S τ-value of ~150–200 s. This linear regime includes practically relevant separator thicknesses (commercial Li ion batteries tend to have separator thicknesses between 20 and 25 μm).[2–4,35] However, for L_S above ~65 μm, τ appears to saturate at a value of ~600 s.

To begin to understand this behaviour, we introduce the physical model mentioned in the introduction. This yields an equation for τ as a function of various physical properties of the cell.[19] This model considers the timescales associated with electron and ionic motion during charge/discharge including: the RC charging time associated with the system, the ion diffusion time within the system and the timescale of the electrochemical reaction (see Ref. 19 for more details). These contributions lead to Eq. 3a which has seven distinct terms. The RC terms are made up of

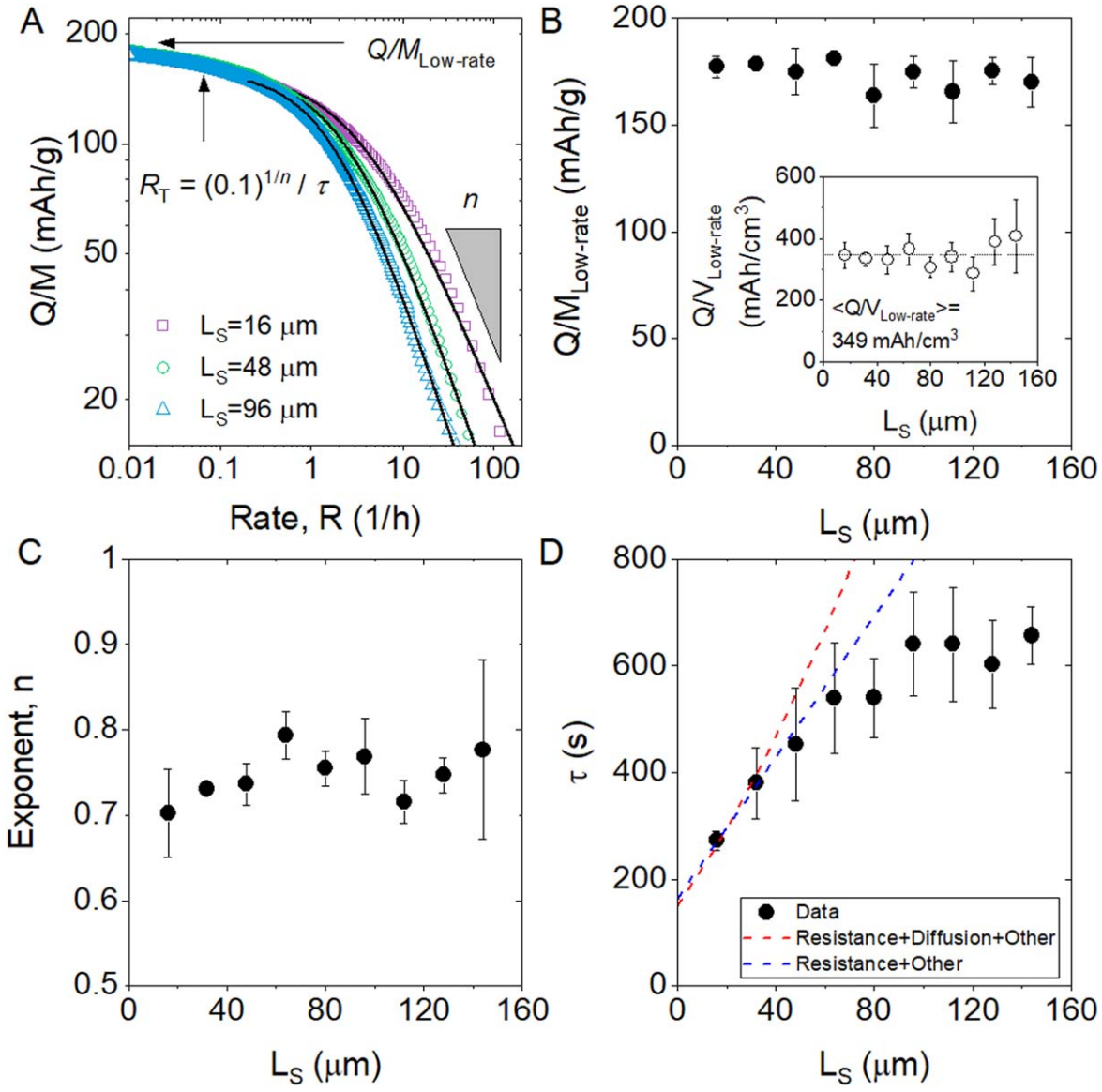

Figure 3. Quantifying the effects of separator thickness (L_S) on rate performance. (A) Specific capacity (Q/M) vs rate (R) curves for three different separator thicknesses as acquired from chronoamperometry. The curves are fitted to Eq. 2, outputting fitting parameters that are used to quantitatively describe rate performance. (B) Low-rate specific capacity, $Q/M_{\text{Low-rate}}$, obtained not from fitting, but from reading off the Q/M value at a rate of $R = 0.01\ \text{h}^{-1}$, plotted as a function of L_S. (C)–(D) Rate exponent, n, (C) and characteristic time, τ, (D) both plotted as a function of L_S. These data were obtained by fitting curves such as those in A to Eq. 2. Figure 3D also shows two fits using Eq. 3b, both applied to only the first 4 data points. The red line fit includes the effect of ionic diffusion in the separator while the blue fit does not.

the electrical resistance of the electrode (term 1) and the ionic resistance of the electrolyte within the pores of the electrode (term 2) and within the separator (term 4). The terms associated with ion diffusion times include the time for ions to diffuse through the electrolyte within the pores of the electrode (term 3) and the pores of the separator (term 5) and the solid-state ion diffusion time (term 6). Lastly, term (7) is associated with the timescale of the electrochemical reaction, t_c. Combining these terms gives the following expression:

$$\tau = L_E^2\left[\frac{C_{V,eff}}{2\sigma_{OOP}} + \frac{C_{V,eff}}{2\sigma_{E,E}} + \frac{1}{D_{E,E}}\right] + L_E\left[\frac{L_S C_{V,eff}}{\sigma_S}\right] + \left[\frac{L_S^2}{D_S} + \frac{L_{AM}^2}{D_{AM}} + t_c\right] \quad [3a]$$

Term 1 2 3 4 5 6 7

Where L_E is the electrode thickness, $C_{V,\text{eff}}$ is the effective volumetric capacitance of the electrode, σ_{OOP} is the out-of-plane electronic conductivity of the electrode, $\sigma_{E,E}$ is the ionic conductivity of the electrolyte within the pores of the electrode, $D_{E,E}$ is the ion diffusion coefficient in the electrolyte within the pores of the electrode. L_{AM} is the solid-state diffusion length (related to active particle size) and D_{AM} is the Li ion diffusion coefficient within the active particles. Note, that D_{AM} is an effective value, averaged over all states of charge. Most relevant for this work, σ_S and D_S are the ionic conductivity and diffusivity of the electrolyte within the separator. In addition, we note that a number of experimental studies have shown the empirical relationship: $C_{V,eff} = (28\text{F mAh}^{-1}) \times (Q/V)_{Low-Rate}$.[16,19,22]

This equation has been shown to describe experimental data very accurately.[19] For example, Eq. 3a was found to match experimental data for τ vs σ_{OOP} extremely well using only literature values for the various electrode parameters.[22] In addition, Eq. 3a was found to closely match experimental data for τ vs L_E.[16]

Considering only the effects of the separator as represented by terms 4 and 5, and using the empirical relation above to replace $C_{V,\text{eff}}$, we can re-write Eq. 3a as:

$$\tau = \Sigma_{1,2,3,6,7} + \frac{28 L_S L_E (Q/V)_{Low-Rate}}{\sigma_S} + \frac{L_S^2}{D_S} \quad [3b]$$

where $\Sigma_{1,2,3,6,7}$ is just the sum of terms 1, 2, 3, 6 and 7 in Eq. 3a. Here the term containing L_S represents the effect of the resistance of the electrolyte within the separator while the term containing L_S^2 represents diffusion of ions within the separator. It is worth noting that the electrode thickness dependent study reported in Ref. 16 showed that electrolyte resistance term (i.e. term 4 in Eq. 3a) cannot be neglected while the sum of terms 5, 6 and 7 in Eq. 3a can be relatively small. This latter factor may be important here as it could mean that the resistance of the electrolyte in the separator (term 4) has a greater impact on rate performance than ionic diffusion within the separator (term 5).

We note that we expect σ_S and D_S to be smaller than the equivalent values in bulk electrolyte (σ_{BL} and D_{BL} respectively) due to the porosity and increased tortuosity within the separator. Generally, we would expect $D_S/D_{BL} = \sigma_S/\sigma_{BL} = P_S/\kappa_S \approx 0.08$ as described above.[29]

Having outlined the model above, the first thing to note is that it cannot explain the saturation of τ at large separator thicknesses. To our knowledge, electrochemical models do not describe this phenomenon either. The effect of electrolyte resistance should result in τ increasing continuously with L_S without saturation while ionic diffusion should lead to a superlinear increase in τ with L_S so long as the concentration gradient spans the entire separator. Thus, the saturation shown in Fig. 3D remains unexplained.

However, the technologically relevant pre-saturation increase shown by the first four τ vs L_S data points can potentially be described by Eq. 3b which predicts a quadratic (i.e. second degree polynomial) behaviour. However, attempts to fit a second order polynomial to the first four data points results in a negative value of D_S which is clearly non-physical. This is simply due to the limited number of data points which is in turn limited by available separator thicknesses. To address this problem, we have fit the first four data points in Fig. 3D with equation 3C allowing only $\Sigma_{1,2,3,6,7}$ as a free parameter. For the other parameters, we use those fixed values of $L_E = 27\ \mu m$, $(Q/V)_{Low-Rate} = 3.5 \times 10^8$ mAh m^{-3} and $\sigma_S = 0.04$ S m^{-1} given above. In addition, we estimate $D_S = 2.4 \times 10^9$ m^2 s^{-1}, using $D_S = D_{BL}\sigma_S/\sigma_{BL}$ with the expected values of $D_{BL} = 3 \times 10^{10}$ m^2 s^{-1} and $\sigma_{BL} = 0.5$ S m^{-1}.[31,36] This fit is shown as the dashed red line and matches the data reasonably well for $L_S < 40\ \mu m$ but clearly diverges for larger separator thicknesses. The fit yields a value of $\Sigma_{1,2,3,6,7} = 150 \pm 20$ s. The divergence of this fit from the data is clearly due to the super-linear contribution of the diffusion term (i.e. L_S^2/D_S). As mentioned above, the data in Ref. 16 suggests that, while the electrolyte resistance contribution (term 4) cannot be neglected, it is still unclear if the ionic diffusion term in Eqs. 3a and 3b (term 5) is necessary.

With this in mind, we also fit the first four data points in Fig. 3D to Eq. 3b but neglecting the ionic diffusion term (i.e. $\tau = \sum_{1,2,3,6,7} + 28 L_S L_E (Q/V)_{Low-Rate}/\sigma_S$). As before, we used the fixed values of L_E, $(Q/V)_{Low-Rate}$ and σ_S given above and set $\Sigma_{1,2,3,6,7}$ as a free parameter. This fit is plotted as the blue solid line and yields $\Sigma_{1,2,3,6,7} = 165 \pm 5$ s. We note that this fit matches the data much more closely in the pre-saturation regime than does the fit including ionic diffusion (red line). This result suggests that the impact of ionic diffusion within the separator on rate performance to be much less important than that of the resistance of the electrolyte within the separator. In fact, it is probably safe to assume that term 5 can be neglected from Eq. 3a with no loss of accuracy.

This is an important result and shows that the increase in τ with L_S can be completely explained via the contribution of the ionic resistance within the separator to the RC charging time of the cell as expressed via Eq. 3a. Indeed, the rate of increase is quantitatively described by Eq. 3a ($d\tau/dL_S = 28 L_E (Q/V)_{Low-Rate}/\sigma_S$) with a high degree of accuracy using no adjustable parameters.

In addition, this result explains why the exponent, n, increases with separator thickness, at least at low L_S. As mentioned above, $n \sim 0.5$ is associated with diffusion limitations while $n \sim 1$ implies electrical limitations. If the rate-limitation associated with the separator is predominately due to electrolyte resistance, then increasing separator thickness increases the contribution of cell resistance to the overall rate limitations. We would expect[16] this to result in an increase in n, as is observed.

Finally, we can check whether the fit values for $\Sigma_{1,2,3,6,7}$ are line with the predictions of Eq. 3a. Taking reasonable values of the various parameters in Eq. 3a (see SI—Supplementary Note 2) yields a value of $\Sigma_{1,2,3,6,7} \sim 100$ s which is in reasonable agreement with the fit value of $\Sigma_{1,2,3,6,7} = 165 \pm 5$ s.

Conclusions

We have measured the effect of separator thickness of the rate-performance using NMC-nanotube composites as a model electrode system. We achieve this quantitatively by using a semi-empirical equation to fit capacity vs rate data, outputting the characteristic time associated with charge/discharge. We find this time to increase approximately linearly with separator thickness, before saturating for thicknesses above $\sim 100\ \mu m$. We analyse the pre-saturation portion of the data using a physical model which expresses the characteristic time in terms of the various physical properties of the cell. This analysis suggests the resistance of the electrolyte within the separator to be the dominant rate-limiting factor with ion diffusion within the separator much less important. We note that the method we have presented here could be used to test the impact of various separator-related parameters on rate capability. For example, one might examine in detail how factors such as separator tortuosity, porosity or pore size quantitatively affect rate capability in batteries.

Acknowledgments

This work was funded by the Science Foundation Ireland (SFI) funded centre AMBER (SFI/12/RC/2278_P2). We acknowledge the facilities of the SFI-funded AML and ARM labs. JNC also thanks the European Research Council (Advanced Grant FUTURE-PRINT) and the European Commission (Graphene Flagship cores 2 & 3, grant agreements 785219 and 881603).

ORCID

Dominik V. Horváth https://orcid.org/0000-0003-2256-6120
Ruiyuan Tian https://orcid.org/0000-0003-1282-1087

References

1. P. Arora and Z. Zhang, "Battery separators." *Chem. Rev.*, **104**, 4419 (2004).
2. J. Jang, J. Oh, H. Jeong, W. Kang, and C. Jo, "A review of functional separators for lithium metal battery applications." *Materials (Basel, Switzerland)*, **13**, 4625 (2020).
3. M. F. Lagadec, R. Zahn, and V. Wood, "Characterization and performance evaluation of lithium-ion battery separators." *Nature Energy*, **4**, 16 (2019).
4. C. M. Costa, Y.-H. Lee, J.-H. Kim, S.-Y. Lee, and S. Lanceros-Méndez, "Recent advances on separator membranes for lithium-ion battery applications: from porous membranes to solid electrolytes." *Energy Storage Mater.*, **22**, 346 (2019).
5. M. F. Lagadec, R. Zahn, S. Müller, and V. Wood, "Topological and network analysis of lithium ion battery components: the importance of pore space connectivity for cell operation." *Energy Environ. Sci.*, **11**, 3194 (2018).
6. I. V. Thorat, D. E. Stephenson, N. A. Zacharias, K. Zaghib, J. N. Harb, and D. R. Wheeler, "Quantifying tortuosity in porous Li-ion battery materials." *J. Power Sources*, **188**, 592 (2009).
7. K. M. Abraham, "Directions in secondary lithium battery research and development." *Electrochim. Acta*, **38**, 1233 (1993).
8. D. Djian, F. Alloin, S. Martinet, H. Lignier, and J. Y. Sanchez, "Lithium-ion batteries with high charge rate capacity: Influence of the porous separator." *J. Power Sources*, **172**, 416 (2007).
9. K. K. Patel, J. M. Paulsen, and J. Desilvestro, "Numerical simulation of porous networks in relation to battery electrodes and separators." *J. Power Sources*, **122**, 144 (2003).
10. J. Cannarella and C. B. Arnold, "Ion transport restriction in mechanically strained separator membranes." *J. Power Sources*, **226**, 149 (2013).

11. E. Lizundia, C. M. Costa, R. Alves, and S. Lanceros-Méndez, "Cellulose and its derivatives for lithium ion battery separators: a review on the processing methods and properties." *Carbohydrate Polymer Technologies and Applications*, **1**, 100001 (2020).
12. J.-L. Pan, Z. Zhang, H. Zhang, P.-P. Zhu, J.-C. Wei, J.-X. Cai, J. Yu, N. Koratkar, and Z.-Y. Yang, "Ultrathin and strong electrospun porous fiber separator." *ACS Appl. Energy Mater.*, **1**, 4794 (2018).
13. R. Pan, Z. Wang, R. Sun, J. Lindh, K. Edström, M. Strømme, and L. Nyholm, "Thickness difference induced pore structure variations in cellulosic separators for lithium-ion batteries." *Cellulose*, **24**, 2903 (2017).
14. S. G. Lim, H. D. Jo, C. Kim, H. T. Kim, and D. R. Chang, "Electro-spun poly (vinylidene fluoride) nanofiber web as separator for lithium ion batteries: effect of pore structure and thickness." *J. Nanosci. Nanotechnol.*, **16**, 956 (2016).
15. D. Djian, F. Alloin, S. Martinet, and H. Lignier, "Macroporous poly(vinylidene fluoride) membrane as a separator for lithium-ion batteries with high charge rate capacity." *J. Power Sources*, **187**, 575 (2009).
16. D. V. Horváth, J. Coelho, R. Tian, V. Nicolosi, and J. N. Coleman, "Quantifying the dependence of battery rate performance on electrode thickness." *ACS Appl. Energy Mater.*, **3**, 10154 (2020).
17. D. Miranda, C. M. Costa, A. M. Almeida, and S. Lanceros-Méndez, "Modeling separator membranes physical characteristics for optimized lithium ion battery performance." *Solid State Ionics*, **278**, 78 (2015).
18. T. F. Fuller, M. Doyle, and J. Newman, "Simulation and optimization of the dual lithium ion insertion cell." *J. Electrochem. Soc.*, **141**, 1 (1994).
19. R. Tian, S.-H. Park, P. J. King, G. Cunningham, J. Coelho, V. Nicolosi, and J. N. Coleman, "Quantifying the factors limiting rate performance in battery electrodes." *Nat. Commun.*, **10**, 1933 (2019).
20. R. Tian, P. J. King, J. Coelho, S.-H. Park, D. V. Horvath, V. Nicolosi, C. O'Dwyer, and J. N. Coleman, "Using chronoamperometry to rapidly measure and quantitatively analyse rate-performance in battery electrodes." *J. Power Sources*, **468**, 228220 (2020).
21. S.-H. Park et al., "High areal capacity battery electrodes enabled by segregated nanotube networks." *Nat. Energy*, **4**, 560 (2019).
22. R. Y. Tian, N. Alcala, S. J. K. O'Neill, D. V. Horvath, J. Coelho, A. J. Griffin, Y. Zhang, V. Nicolosi, C. O'Dwyer, and J. N. Colemand, "Quantifying the effect of electronic conductivity on the rate performance of nanocomposite battery electrodes." *ACS Appl. Energy Mater.*, **3**, 2966 (2020).
23. C. Heubner, C. Lämmel, A. Nickol, T. Liebmann, M. Schneider, and A. Michaelis, "Comparison of chronoamperometric response and rate-performance of porous insertion electrodes: towards an accelerated rate capability test." *J. Power Sources*, **397**, 11 (2018).
24. J. W. Fergus, "Recent developments in cathode materials for lithium ion batteries." *J. Power Sources*, **195**, 939 (2010).
25. J. B. Boland et al., "Liquid phase exfoliation of GeS nanosheets in ambient conditions for lithium ion battery applications." *2D Mater.*, **7**, 035015 (2020).
26. V. Vega-Mayoral, R. Tian, A. G. Kelly, A. Griffin, A. Harvey, M. Borrelli, K. Nisi, C. Backes, and J. N. Coleman, "Solvent exfoliation stabilizes TiS_2 nanosheets against oxidation, facilitating lithium storage applications." *Nanoscale*, **11**, 6206 (2019).
27. M. S. Whittingham, "Lithium batteries and cathode materials." *Chem. Rev.*, **104**, 4271 (2004).
28. X. Li, J. Liu, M. N. Banis, A. Lushington, R. Li, M. Cai, and X. Sun, "Atomic layer deposition of solid-state electrolyte coated cathode materials with superior high-voltage cycling behavior for lithium ion battery application." *Energy Environ. Sci.*, **7**, 768 (2014).
29. D.-W. Chung, M. Ebner, D. R. Ely, V. Wood, and R. Edwin García, "Validity of the Bruggeman relation for porous electrodes." *Model. Simul. Mater. Sci. Eng.*, **21**, 074009 (2013).
30. F. L. E. Usseglio-Viretta et al., "Resolving the discrepancy in tortuosity factor estimation for Li-Ion battery electrodes through micro-macro modeling and experiment." *J. Electrochem. Soc.*, **165**, A3403 (2018).
31. E. R. Logan, E. M. Tonita, K. L. Gering, J. Li, X. Ma, L. Y. Beaulieu, and J. R. Dahn, "A study of the physical properties of li-ion battery electrolytes containing esters." *J. Electrochem. Soc.*, **165**, A21 (2018).
32. J. N. Coleman and R. Y. Tian, "Developing models to fit capacity-rate data in battery systems." *Current Opinion in Electrochemistry*, **21**, 1 (2020).
33. R. Tian, M. Breshears, D. V. Horvath, and J. N. Coleman, "The rate performance of two-dimensional material-based battery electrodes may not be as good as commonly believed." *Acs Nano*, **14**, 3129 (2020).
34. J. N. Coleman and R. Tian, "Developing models to fit capacity–rate data in battery systems." *Current Opinion in Electrochemistry*, **21**, 1 (2020).
35. C. M. Costa, M. M. Silva, and S. Lanceros-Méndez, "Battery separators based on vinylidene fluoride (VDF) polymers and copolymers for lithium ion battery applications." *RSC Adv.*, **3**, 11404 (2013).
36. A. Ehrl, J. Landesfeind, W. A. Wall, and H. A. Gasteiger, "Determination of transport parameters in liquid binary lithium ion battery electrolytes." *J. Electrochem. Soc.*, **164**, A826 (2017).